Journal of Mechanical Engineering and Sciences
ISSN (Print): 2289-4659; e-ISSN: 2231-8380
Volume 13, Issue 4, pp. 6088-6111, December 2019

DOI: https://doi.org/10.15282/jmes.13.4.2019.23.0479

Thermodynamic and exergic modelling of a combined cooling, heating and power system based on solid oxide fuel cell

J. Pirkandi[1], A. M. Joharchi[2] and M. Ommian[1]

[1] Faculty of Aerospace Engineering, Malek Ashtar University of Technology
15875-1774, Tehran, IRAN
*Email: jpirkandi@mut.ac.ir
Phone: +982122945141; Fax: +982122935341
[2] Faculty of Mechanical Engineering, West Branch of Azad University
1468763785, Tehran, IRAN

ABSTRACT

In this research, thermodynamic and exergic analyses have been carried out on a combined cooling, heating and power cogeneration system that includes a solid oxide fuel cell and a single-effect lithium bromide absorption chiller. Results indicate that by increasing the system inlet air flow rate, the overall efficiency of the hybrid system is reduced, due to the reduction of the cell's working temperature and exhaust gases temperature; while an increase in the working pressure of the system has no effect on its efficiency. The results also show that by raising the temperature of exhaust gases, the rate of exergy destruction diminishes, while the rate of exergy loss in the hybrid system increases. In the absorption chiller cycle, the maximum exergy destruction rate occurs in the generator, and the minimum rate is achieved in the pressure-reducing valve, between the evaporator and the condenser. Also, in the fuel cell cycle, the highest exergy destruction rate occurs in the heat exchanger of the inlet air to the cell, and the lowest exergy destruction rate occurs in the two water pumps. Moreover, the entropy generation rate and the exergy destruction rate of the fuel cell cycle are higher than those of the chiller cycle.

Keywords: Solid oxide fuel cell; absorption chiller; entropy; exergy.

INTRODUCTION

Cogeneration Systems are systems that can generate several forms of energy using a primary source of energy. These systems, if properly designed and operated, can save energy, because it is more efficiency compare to a single system of electricity and heat. Reducing emissions, lower noise and high efficiency are the main benefits of cogeneration systems [1]. This equipment consists of three main components: primary actuator, thermal recovery and a cooling system. Primary actuators in these systems often include gas turbines (microturbines), internal combustion engines, sterilizing motors and fuel cells. Having a reliable, low-cost, and affordable energy production system has introduced the use of fuel cells as an important candidate [2].

In fuel cell, hydrogen produces electrical power during a series of electrochemical reactions with oxygen, is one of the best alternatives for generating energy in cogeneration systems. Fuel cells due to high efficiency, non-emission of environmental pollutants, high power potential, lack of moving parts, lack of vibration and low noise are the desirable equipment for energy production. One of the most important and useful types of fuel cells is a solid oxide fuel cell. The high operating temperature of these fuel cells (800 to 1000 degrees Celsius) has led to the use of various fuels, such as natural gas. In addition, the heat generated in this type of fuel cell is of high quality and can be used in most of the cogeneration systems [3].

One of the uses of solid oxide fuel cells is the combination of these types of cells with different types of absorption chillers [4]. Absorption chillers are devices that require a high temperature heat source to generate refrigeration. If cheap energy sources are available (temperatures range 100 to 200 degrees Celsius), these types of chillers are very economical. Absorption chillers are widely used in residential and commercial buildings as a source of cooling products in air-conditioned systems. In absorption systems, heat from a heat source (hot water or steam) should be transferred into generator. The use of a solid oxide fuel cell makes the hot gases from the outlet able to supply the generator's heat [3]. The fuel cell used in this type of hybrid system, in addition to providing the heat required by the generator, can also provide part of the electrical power and the hot water of the building. The schematic of a hybrid system consisting of a solid oxide fuel cell and an absorbing chiller of lithium bromide is shown in Figure 1, its efficiency is estimated at 87%.

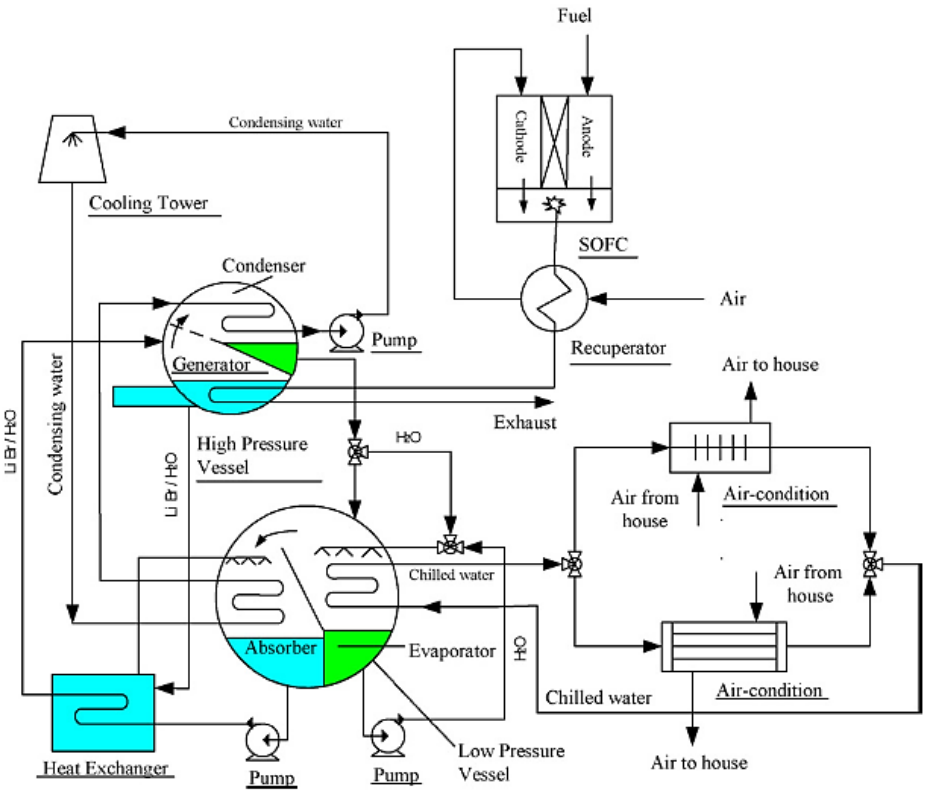

Figure 1. A view of solid oxide fuel cell and absorption chiller combined cycle.

In recent years, many scientific studies have been conducted on the Simultaneous production of electricity, heat and refrigeration. Reviews and researches show that hybrid fuel cell and chiller absorption systems have been less studied and more research has been done on other systems such as gas turbine and chiller absorption.

Velumani et al. [5] proposed and analyzed a CHP hybrid system for a 230kW demand building. The system investigated the coupling of a 200 kW Solid Oxide Fuel Cell stack, 30 kW Microturbine and a single effect Absorption cooling system providing 55 kW for air conditioning using water chillers. Ozcan et al. [6] presented assessment of thermodynamic performance through exergy and energy analysis for heating, cooling and power hybrid system. In this research parametric study is performed for impact of system parameters and environmental condition on performance of hybrid system. Ranjbar et al. [7] presented novel tri-generation hybrid system based on a solid oxide fuel cell (SOFC). This hybrid system includes a generator-absorber heat exchanger for cooling and a heat exchanger for the heating process. The influences of current density and inlet flow temperature on several variables are investigated. Zhao et al. [8] used flue gas exhausted for heating of water exhausted from the steam turbine is used for cooling achieved by a single-effect lithium bromide absorption chiller and evaluated system performance by Aspen Plus process simulator. Chitsaz et al. [9] modeled and analyzed exergo-economic of a tri-generation system based on a solid oxide fuel. In this study, effects of current density, inlet flow temperature and fuel utilization factor are investigated on several variables include unit cost of the electrical power, unit cost of the cooling, unit cost of the heating and total unit cost of the products. Moussawi et al. [10] selected and designed tri-generation system based on solid oxide fuel cell (SOFC) for domestic applications. The system was founded on three stages including: the energy simulation of residential building, the system's prime mover–SOFC, and the trigeneration recovery system ensuring the maximum coverage of heating, cooling, and domestic hot water loads respectively. Jing et al. [11] evaluated from different perspectives the feasibility of solid oxide fuel cell based combined cooling heating and power (SOFC-CCHP) applications. On the other hand, simulated operations of the natural gas fuelled SOFC-CCHP systems for several locations. Jing et al. [12] developed hybrid system based on SOFC-CCHP and operation optimization model using the Mixed Integer Non-linear Programming approach. The model provides two capacity sizing options of the fixed size, and the optimal sizing. Qinlong Hou et al. [13] investigated a distributed energy system based on solar methanol reforming SOFC which combine GT-ST power generation system with AHP-AR and the performance analysis of SOFC integrated system is carried out which reveals the affinity of solar energy and chemical energy.

This paper has introduced a hybrid system based on solid oxide fuel cell and lithium bromide single-effect absorption chiller for cogenerating cooling, heating and electricity. First, the considered hybrid system and its auxiliary equipment have been described and then full thermodynamic and exergic analyses have been performed for all the considered cycle components. Contrary to most previous research works, in this paper, the computations pertaining to fuel cell have been carried out separately for three different areas, including the computations related to the reforming, electrochemical, and thermal sections. Also, the absorption chiller used in this research has been completely modelled and all its components have been analyzed. Then, through a parametric study of the mentioned hybrid system, the effects of the molar flow rate of system inlet air, working pressure ratio of compressor and the temperature of exhaust gases on the working temperature of fuel cell, overall system

efficiency, and on the rates of exergy destruction and loss in the system have been investigated. Finally, an optimal operating state has been presented for the proposed system.

INTRODUCING THE PROPOSED SYSTEM

The schematic of the hybrid system studied in this research has been depicted in Figure 2. The proposed system consists of a solid oxide fuel cell stack with internal reforming, an afterburner chamber, an air compressor, a fuel compressor, two water pumps, four recuperators and a single-effect lithium bromide absorption chiller. The ambient air coming into the system is compressed first by the air compressor and after passing through the first thermal recuperator and getting heated, it enters the cathode section of the fuel cell at a high temperature. Also, the fuel used in the system is compressed first by the fuel compressor, preheated in the second recuperator and then sent to the anode section of the fuel cell. The electrochemical reactions taking place within the cell generate electricity and thermal energy. The leftover air and fuel then enter the afterburner chamber and are combusted there. The exhaust gases from the afterburner, which have high temperature and energy, are conveyed toward the four mentioned system recuperators. After preheating the cell inlet air and fuel, these gases enter two other heat recuperators. The main function of the last two recuperators is to produce hot water for the absorption chiller generator and also for the heating systems.

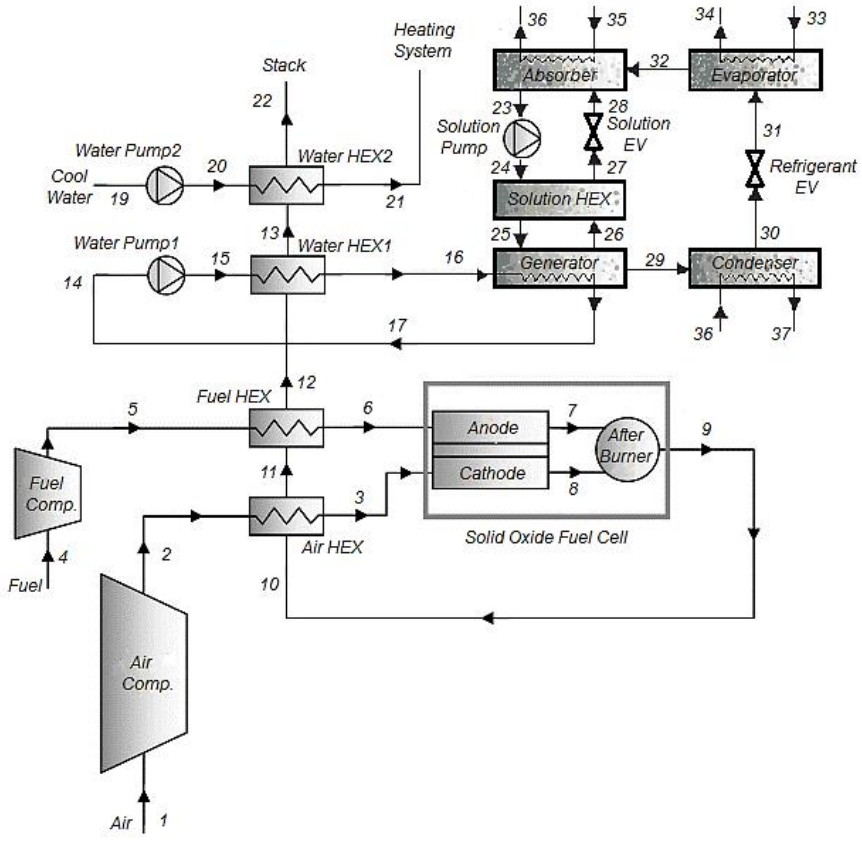

Figure 2. Schematic of solid oxide fuel cell and absorption chiller.

ASSUMPTIONS

Some assumptions have been considered in modelling and analyzing of hybrid systems:

- Gas leakage from inside the system to the outside has been ignored.
- The fuel used in the system is natural gas (methane).
- A stable fluid flow has been considered in all the cycle components.
- Changes in kinetic energy and potential are neglected.
- The behavior of all gases in the cycle is assumed to be ideal gas.
- Within the fuel cell, the distribution of pressure, temperature and chemical components has been disregarded.
- The temperature of the anode and cathode outlets is the same and equal to the working temperature of the cell.
- For the cells of the fuel cell, a constant voltage has been considered
- It has been assumed that the fuel inside the fuel cell converts to hydrogen through internal reforming.
- The refrigerant (water) is assumed to be saturated liquid at the outlet of condenser and saturated vapor at the outlet of evaporator.
- The solution of lithium bromide is assumed to be at dilute solution at the outlet of absorber and is located at the temperature of the absorber.
- The output temperature of the refrigerant and solution from the generator is equal to the generator temperature.
- The pipeline pressure drop from the output of the chiller generator to the inlet of the pump is 7%.
- The cooling water of the chiller directly enters the condenser after passing through the absorber.
- The reference values for the ambient are 25 °C temperature and 1 bar atmospheric pressure and 50% concentration.

GOVERNING EQUATIONS

Firstly by employing the existing equations, the performances of all the components of the hybrid system are defined and then under stable conditions, the above system is reviewed and analyzed.

Absorption Chiller

The absorption chiller is made up of four important components including a generator, a condenser, an evaporator and an absorber. Absorption chillers use water as a cooling fluid and lithium bromide as an absorber. By reducing the pressure within the evaporator to one-hundredth of an Atmosphere (complete vacuum), the water inside evaporates at temperature 5.4 ºC. The evaporation process, due to its endothermic nature, cools a portion of the remaining water inside the evaporator to lower than 5.4 ºC. In order to use the cooling generated in the evaporator, a coil can be installed inside it. Since water boils at 5.4 ºC when the pressure is 0.01 atm, the temperature of cold water in cooling and ventilation systems can be lowered to 5.6 ºC. The water vapor produced in the evaporator goes to the absorber and is

absorbed by the lithium bromide solution. As this process continues, the lithium bromide solution becomes diluted and can no longer absorb the water [14]. To solve this problem, the diluted solution of lithium bromide is pumped to the generator and, there, it is indirectly heated by the hot water. This heating causes the lithium bromide solution to boil, thereby releasing the water vapor from it. The concentrated lithium bromide solution is conveyed to the absorber so that it can again absorb more water vapor. The water vapor thus extracted in the generator enters the condenser unit and is condensed there. This condensed water is sent back to the evaporator to restart the process, and thus a closed cycle is formed. The energy balance equations for the single-effect absorption chiller components, shown in Figure 2, are as follows:

Generator

The generator's main function is to heat the dilute solution of lithium bromide and to extract the water vapor from it [14].

$$Q_{gen} = m_{26}h_{26}+m_{29}h_{29} - m_{25}h_{25} \quad (1)$$

$$Q_{gen} = m_{17}c_p(T_{16} - T_{17}) \quad (2)$$

In the above equation, Q_{gen} is the heat transferred to the generator from the warm water produced in the third recuperator.

Condenser

The main function of the condenser is to cool and condense the water vapor produced.

$$Q_{cond} = m_{29}h_{29} - m_{29}h_{30} \quad (3)$$

$$Q_{cond} = m_{36}c_p(T_{37} - T_{36}) \quad (4)$$

In the above equation, Q_{cond} denotes the amount of heat transferred by the condenser to the cooling water in the cycle. Normally, the cooling water is circulated in the cycle by means of a cooling tower. This water enters the absorber and then the condenser at a temperature of 30 ºC and after absorbing heat from the condenser, leaves it at a temperature of 35 ºC [14].

Evaporator

The evaporator is mainly used to produce cooling energy in the absorption cycle.

$$Q_{eva} = m_{32}h_{32} - m_{31}h_{31} \quad (5)$$

$$Q_{eva} = m_{33}c_p(T_{33} - T_{34}) \quad (6)$$

In the above equation, Q_{eva} denotes the amount of heat transferred from the water in the cooling system to the evaporator. This water usually enters the evaporator at temperature 12-13 ºC and leaves it at 6-7 ºC. This water is ordinarily used in fan coil or air conditioning units for building cooling [8].

Absorber

This unit absorbs the water vapor produced in the evaporator [14].

$$Q_{abs} = m_{28}h_{28}+m_{32}h_{32} - m_{23}h_{23} \quad (7)$$

$$Q_{abs} = m_{36}c_p(T_{36} - T_{35}) \quad (8)$$

In the above equation, Q_{abs} is the amount of heat transferred from the absorber to the cooling water. As it was pointed out in the section related to condenser, this water enters the absorber at temperature 35 ºC and after cooling the lithium bromide solution there, it goes to the

condenser to absorb heat again. Cooling the lithium bromide solution increases its water vapor absorption capacity [14].

Pump

The pump is used to convey the diluted lithium bromide solution from the absorber to the generator [8].

$$W_p = m_{24}\vartheta_{24}\,(P_{24} - P_{23})/\eta_p \tag{9}$$

$$W_p = m_{23}\,(h_{24} - h_{23}) \tag{10}$$

In the above equation, W_p represents the mechanical work done by the pump. Considering the above equations, in this section, the performance coefficient of the chiller is expressed as:

$$COP_{chiller} = \frac{Q_{eva}}{Q_{gen}+W_P} \tag{11}$$

Also, the exergic efficiency of the chiller is obtained through Equation. (12):

$$\psi_{chiller} = \frac{Q_{eva}\cdot\left(1-\frac{T_0}{T_b}\right)}{\left[Q_{gen}\cdot\left(1-\frac{T_0}{T_h}\right)+Wp\right]} \tag{12}$$

In this equation T_b is the average temperature of the cold source (in the evaporator) and T_h is the average temperature of the hot source (in the generator).

Fuel Cell

The equations pertaining to fuel cell have been presented in three parts, including the electrochemical, thermal, and thermodynamic equations. The reversible voltage of fuel cell is obtained by Nernst equation (Equation. (13)) [15]:

$$E = E^{\circ} + \frac{R_u T}{n_e F}\ln\left(\frac{P_{H_2}P_{O_2}^{1/2}}{P_{H_2O}}\right) \tag{13}$$

To compute the actual cell voltage, the losses associated with the cell, including the activation voltage loss (V_{act}), ohmic voltage loss (V_{ohm}) and the concentration voltage loss (V_{conc}) should be determined and used in Equation. (14) to get the real cell voltage (V_{cell}) [15]:

$$V_{cell} = E - (V_{act}+V_{ohm}+V_{conc}) = E - \Delta V_{loss} \tag{14}$$

The chemical reactions taking place in a fuel cell are exothermic processes. The amount of heat transfer in a process is obtained by writing the thermodynamic equation between reactants and the resulting products. The heat released from the chemical reaction in the fuel cell can be calculated according to Equation. (15) [15]:

$$\dot{Q}_{elec} = zT\Delta S - I\Delta V_{loss} \tag{15}$$

The net leftover heat from the chemical reactions in the fuel cell is obtained from Equation. (16):

$$\dot{Q}_{net} = \dot{Q}_{elec} \tag{16}$$

Some of this net residual heat is spent to raise the temperature of cell's internal and exhaust gases ($\dot{Q}'$) and some of it is released to the surrounding ($\dot{Q}_{surr}$).

$$\dot{Q}_{net} = \dot{Q}' + \dot{Q}_{surr} \tag{17}$$

$$\dot{Q}_{net} = (\dot{n}_6 h_6 - \dot{n}_7 h_7)_{an} + (\dot{n}_3 h_3 - \dot{n}_8 h_8)_{ca} + \dot{Q}_{surr} \tag{18}$$

In real situations, the chemical processes within a fuel cell always lose some heat to the surrounding environment. By considering this process as an ideal one, it is assumed that the

fuel cell used is internally adiabatic and that the net residual heat is spent to raise the temperature of cell's internal and exhaust gases ($\dot{Q}''$).

$$\dot{Q}_{elec}=zT\Delta S - I\Delta V_{loss} \tag{19}$$

$$\dot{Q}''=\Delta h_{c.in}+\Delta h_{c.out}+\Delta h_{a.in}+\Delta h_{a.out} \tag{20}$$

An iterative algorithm has been used to compute the temperature of the fuel cell's exhaust gases, and the convergence criterion has been considered as Equation. (21) [15].

$$Q_{error}=\left|\frac{\dot{Q}''-\dot{Q}'}{\dot{Q}'}\right|<0.01 \tag{21}$$

After determining the temperature of exhaust gases, the energy balance equation can be used to calculate the rates of heat losses in the fuel cell.

$$\left(\dot{n}_3\bar{h}_3+\dot{n}_6\bar{h}_6\right)=\dot{Q}_{loss.SOFC}+\dot{W}_{SOFC}+\left(\dot{n}_7\bar{h}_7+\dot{n}_8\bar{h}_8\right) \tag{22}$$

By knowing the fuel utilization coefficient (U_f), the power generation capacity of the fuel cell ($\dot{W}_{SOFC}$) and the net residual heat remaining from cell reactions ($\dot{Q}_{surr}$), the electrical and the thermal efficiencies of the fuel cell are obtained from Equations. (23) and (24), respectively.

$$\eta_{elec.SOFC}=\frac{\dot{W}_{SOFC}}{\dot{n}_f\times LHV\times U_f} \tag{23}$$

$$\eta_{th.SOFC}=\frac{\dot{Q}_{loss.SOFC}}{\dot{n}_f\times LHV\times U_f} \tag{24}$$

Also, the entropy generation rate, exergy destruction rate and the exergic efficiency of the fuel cell are obtained according to the following equations [15]:

$$\dot{S}_{gen.SOFC}=(\dot{n}_7\bar{s}_7+\dot{n}_8\bar{s}_8)-(\dot{n}_3\bar{s}_3+\dot{n}_6\bar{s}_6)+\frac{\dot{Q}_{loss.SOFC}}{T_{surr}} \tag{25}$$

$$\dot{E}_{D.SOFC}=\dot{E}_3+\dot{E}_6-\dot{E}_7-\dot{E}_8-\dot{E}_Q-\dot{W}_{SOFC} \tag{26}$$

$$\psi_{SOFC}=\frac{\dot{W}_{SOFC}}{\dot{E}_3+\dot{E}_6-\dot{E}_7-\dot{E}_8} \tag{27}$$

Compressor

Since isentropic efficiency is dependent on pressure ratio, and a variable pressure ratio has been considered in this modelling, instead of isentropic efficiency, polytropic efficiency ($\eta_{p.ca}$) is used here for the compressor (Equation. (28)), and the temperature of exhaust air is obtained from Equation. (29) [15].

$$\eta_{is.ca}=\frac{(r_{p.ca})^{\frac{k_a-1}{k_a}}}{(r_{p.ca})^{\frac{k_a-1}{k_a\eta_{p.ca}}}} \tag{28}$$

$$\frac{T_2}{T_1}=\left(r_{p,ca}\right)^{\frac{k_a-1}{k_a\eta_{p.ca}}} \tag{29}$$

Using the calculated exhaust air temperature and knowing the temperature and mass flow rate of inlet air, the work done by the compressor is computed according to Equation. (30).

$$\dot{W}_{ca}=\dot{n}_a\left(\bar{h}_2-\bar{h}_1\right) \tag{30}$$

Also, the entropy generation rate, exergy destruction rate and the exergic efficiency for the compression process are obtained according to the following equations [15]:

$$\dot{S}_{gen.ca}=\dot{n}_a.(\bar{s}_2-\bar{s}_1) \tag{31}$$

$$\dot{E}_{D.ca}=\dot{W}_{ca} - (\dot{E}_2 - \dot{E}_1) \quad (32)$$

$$\psi_{ca}=\frac{\dot{E}_2-\dot{E}_1}{\dot{W}_{ca}} \quad (33)$$

In this research, the same temperature has been considered for system inlet air and fuel, and the compressor pressure ratios are such that they provide sufficient working pressure for the fuel cell.

Afterburner

Since only a portion of the air and fuel that enter the system are used up in the fuel cell, it is necessary to have an afterburner chamber for the cycle. The exhaust gases from the fuel cell, including water vapor, carbon dioxide, hydrogen, methane and carbon monoxide in the anode section and unused oxygen and nitrogen in the cathode, react together in the afterburner chamber according to the following equations:

$$CO + \frac{1}{2}O_2 \rightarrow CO_2 \quad , \quad H_2 + \frac{1}{2}O_2 \rightarrow H_2O \quad , \quad CH_4 + 2O_2 \rightarrow CO_2 + 2H_2O \quad (34)$$

All the above reactions are exothermic and they raise the temperature of the gases exiting the afterburner chamber. By writing the energy conservation equation and considering the chamber efficiency, the temperature of exhaust gases can be determined from the following equation [15]:

$$\dot{n}_7\bar{h}_7 + \dot{n}_8\bar{h}_8 - \dot{n}_9\bar{h}_9 - \dot{Q}_{Loss,ab} = 0 \quad (35)$$

In the above equation, $\dot{Q}_{loss,ab}$ denotes the heat losses from the afterburner chamber and its quantity depends on chamber efficiency (η_{ab}), coefficient of fuel utilization in the fuel cell (U_f) and the thermal value of fuel (LHV) [15].

$$\dot{Q}_{Loss,ab} = \dot{n}_4 \times (1 - U_f) \times (1 - \eta_{ab}) \times LHV \quad (36)$$

The entropy generation rate, exergy destruction rate, and the exergic efficiency for the afterburner chamber are determined according to the following equations [15]:

$$\dot{S}_{gen,ab} = \dot{n}_9\bar{s}_9 - \dot{n}_7\bar{s}_7 - \dot{n}_8\bar{s}_8 + \frac{\dot{Q}_{Loss.ab}}{T_{surr}} \quad (37)$$

$$\dot{E}_{D.ab} = \dot{E}_7 + \dot{E}_8 - \dot{E}_9 - \dot{E}_{Q,ab} \quad (38)$$

$$\Psi_{ab} = \frac{\dot{E}_9}{\dot{E}_7 + \dot{E}_8} \quad (39)$$

Recuperators

In this research, four external recuperators, which are supplied by the hot exhaust gases from the fuel cell, have been used for raising the temperature of air and fuel that come into the cell and also for providing the warm water needed by the chiller and the heating system. Based on the efficiency or the performance coefficient of recuperators, the temperatures of exhaust gases from the first and second recuperators are determined according to Equation. (40) and Equation. (41), respectively [15].

$$\varepsilon_{req,1} = \frac{T_3 - T_2}{T_{10} - T_2} \quad (40)$$

$$\varepsilon_{req,2} = \frac{T_6 - T_5}{T_{11} - T_5} \quad (41)$$

By considering the efficiencies of the third and fourth recuperators, the following equations are used to compute the useful thermal load in these recuperators. Also, by using Equation. (43), the amount of warm water needed for the cooling system can be calculated [15].

$$Q_{req,3} = \varepsilon_{req,3} \cdot \dot{n}_{12}(\bar{h}_{12} - \bar{h}_{13}) \quad (42)$$

$$Q_{req,3} = \dot{n}_{water}.\bar{c}_p.(T_{16} - T_{15}) \quad (43)$$

$$Q_{req,4} = \varepsilon_{req,4}\ .\dot{n}_{12}(\bar{h}_{13} - \bar{h}_{22}) \quad (44)$$

$$Q_{req,4} = \dot{n}_{water}.\bar{c}_p.(T_{21} - T_{20}) \quad (45)$$

The entropy generation rate, exergy destruction rate, and the exergic efficiency for the first recuperator can be obtained from the following equations [15]:

$$\dot{S}_{gen,req1} = \dot{n}_2(\bar{s}_3 - \bar{s}_2) - \dot{n}_{10}(\bar{s}_{10} - \bar{s}_{11}) \quad (46)$$

$$E_{D,req1} = (\dot{E}_{10} - \dot{E}_{11}) - (\dot{E}_3 - \dot{E}_2) \quad (47)$$

$$\Psi_{req1} = \frac{\dot{E}_3 - \dot{E}_2}{\dot{E}_{10} - \dot{E}_{11}} \quad (48)$$

Modelling the Pumps

For providing the water pressure in the third and fourth recuperators, two pumps have been used in order to supply the pressure needed by the cooling and heating system. The work done by the third pump is obtained based on the following equation [15]:

$$\dot{W}_{wp1} = \dot{n}_{water}.v_{14}.(P_{15} - P_{14}) \quad (49)$$

Also, the entropy generation rate, exergy destruction rate and the exergic efficiency for the pumps are obtained according to the following equations [15]:

$$\dot{s}_{gen.wp1} = \dot{n}_{w1}.(s_{15} - s_{14}) \quad (50)$$

$$\dot{E}_{D.wp1} = \dot{W}_{wp1} - (\dot{E}_{15} - \dot{E}_{14}) \quad (51)$$

$$\Psi_{wp1} = \frac{\dot{E}_{15} - \dot{E}_{14}}{\dot{W}_{wp1}} \quad (52)$$

System Modelling

In this section, by considering the whole hybrid system as a control volume, the electrical, thermal, overall, and exergic efficiencies are obtained from the following equations [15]:

$$\eta_{elec} = \frac{\dot{W}_{net}}{(\dot{n}_f + \dot{n}_{fi}) \times LHV} \quad (53)$$

$$\eta_{the} = \frac{Q_{req4}}{(\dot{n}_f + \dot{n}_{fi}) \times LHV} \quad (54)$$

$$\eta_{chp} = \frac{\dot{W}_{net} + Q_{req4}}{(\dot{n}_f + \dot{n}_{fi}) \times LHV} \quad (55)$$

$$\eta_{cchp} = \frac{\dot{W}_{net} + Q_{eva} + Q_{req4}}{(\dot{n}_f + \dot{n}_{fi}) \times LHV} = \eta_{elec} + \eta_{the} + \frac{Q_{req4}}{(\dot{n}_f + \dot{n}_{fi}) \times LHV} \quad (56)$$

$$\eta_{exergy.tot} = \frac{\dot{W}_{net} + Q_{eva}(1 - \frac{T_0}{T_b}) + \dot{E}_{21}}{\dot{E}_1 + \dot{E}_4 + \dot{E}_{19}} \quad (57)$$

$\dot{n}_f$ is the flow rate of fuel entering the fuel compressor and $\dot{n}_{fi}$ is the flow rate of fuel entering the afterburner.

SOLUTION ALGORITHM

The governing equations for the components of the absorption chiller and fuel cell cycles have been modelled in the EES software program. In the first part of this program, the information related to the fuel cell cycle (e.g., working pressure ratio of compressor, cycle

inlet air flow rate, temperatures of turbine inlet gases, fuel cell specification, etc.) and the absorption chiller cycle (e.g., temperatures of evaporator, condenser, absorber, generator, etc.) are entered into the program. Then the computations pertaining to the whole hybrid cycle are carried out by guessing an initial working temperature for the fuel cell, and the iterative procedure continues until the set convergence conditions are satisfied (Figure 3).

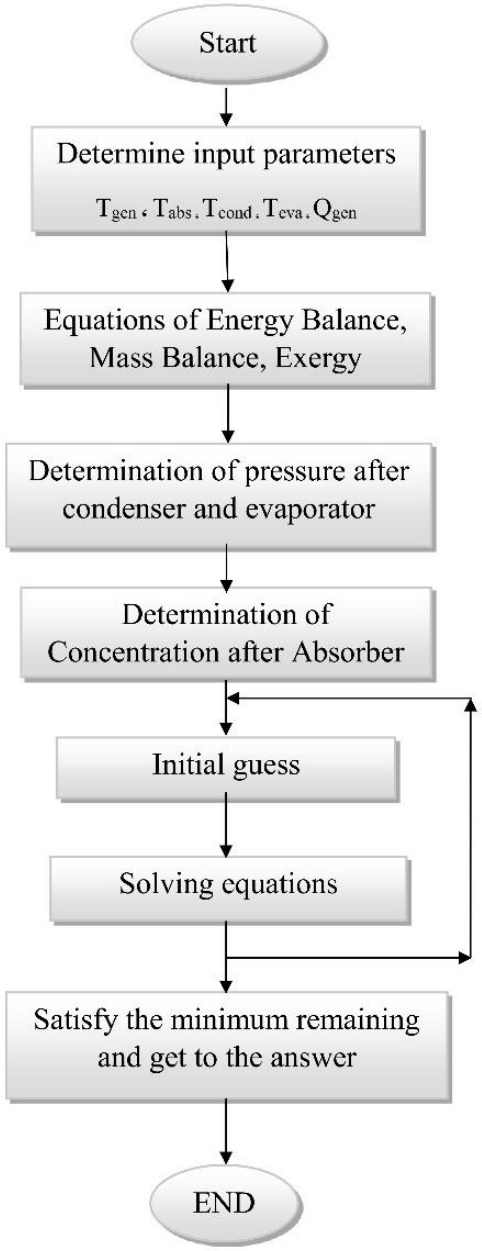

Figure 3. Algorithm for the hybrid system.

The constant values used for the mentioned hybrid system have been given in Table 1.

Table 1. Constant system input values.

Parameter	Assumed value	Parameter	Assumed value
Pump's efficiency (%)	95	Evaporator temperature (T_{eva}) [^{0}C]	<10 $T_{eva} < 4$
Afterburner chamber's efficiency (%)	95	Condenser temperature (T_{cond}) [^{0}C]	<39 $T_{cond} < 33$
Generator's efficiency (%)	95	Absorber temperature (T_{abs}) [^{0}C]	<39 $T_{abs} < 33$
The air-gas recuperator's efficiency (%)	80	Generator temperature (T_{gen}) [^{0}C]	<135 $T_{gen} < 65$
The water-gas recuperator's efficiency (%)	85	Condenser water inlet temperature [^{0}C]	T_{cond} -8
Compressor's isentropic efficiency (%)	81	Condenser water outlet temperature [^{0}C]	T_{cond} -3
Turbine's isentropic efficiency (%)	84	Evaporator water inlet temperature [^{0}C]	T_{eva} +8
Pressure loss of air-gas recuperators (%)	4	Evaporator water outlet temperature [^{0}C]	T_{eva} +3
Pressure loss of water-gas recuperators (%)	4	Generator water inlet temperature [^{0}C]	T_{gen} +18
Pressure loss of afterburner (%)	5	Generator water outlet temperature [^{0}C]	T_{gen} +8
Pressure loss of chiller components (%)	3	Absorber water inlet temperature [^{0}C]	T_{cond} -8
Q_{eva} (kW)	300	Absorber water outlet temperature [^{0}C]	T_{cond} -3

RESULTS AND DISCUSSION

Validation

In this section, the research findings of Rabah Gomri [14] have been used to verify the obtained results. In [14], two single-effect and double-effect absorption chillers have been explored and analyzed from a thermodynamic perspective. For validating the present research results, a single-effect absorption chiller has been modelled with the same inputs considered in Rabah Gomri's research; and the results obtained in the two works have been compared with each other. It should be mentioned that in this modelling, the same working temperature has been assumed for the absorber and the condenser. Also, the cooling water of the considered cycle enters the absorber and the condenser units of the chiller from the cooling tower. The results obtained for the hot water lithium bromide single-effect absorption chiller have been presented in Table 2. This table contains the performance coefficients of the mentioned chiller at several generator temperatures and four different evaporator temperatures. By comparing between the findings of Rabah Gomri and the results obtained from the present modelling, the validity of the results obtained in this research can be easily confirmed.

Table 2. Comparison of the coefficient of performance for the hot water lithium bromide single effect absorption chiller at T_{cond} = 33 °C.

	T_{eva} = 6 [^{0}C]			T_{eva} = 4 [^{0}C]		
T_{gen} [^{0}C]	**Results of Gomri [14]**	**Results of present work**	**Error (%)**	**Results of Gomri [14]**	**Results of present work**	**Error (%)**
75	0.75	0.784	4.5	0.74	0.7604	2.7
85	0.77	0.791	2.7	0.76	0.7785	2.4
95	0.77	0.787	2.2	0.76	0.7786	2.4
105	0.76	0.785	3.2	0.75	0.7777	3.7
	T_{eva} = 10 [^{0}C]			T_{eva} = 8 [^{0}C]		
T_{gen} [^{0}C]	**Results of Gomri [14]**	**Results of present work**	**Error (%)**	**Results of Gomri [14]**	**Results of present work**	**Error (%)**
75	0.78	0.817	4.7	0.77	0.802	4.1
85	0.79	0.812	2.7	0.775	0.801	3.3
95	0.78	0.805	3.2	0.775	0.796	2.7
105	0.775	0.799	3.1	0.77	0.792	2.8

Parametric Analysis of the Absorption Chiller

Considering the important role of the absorption chiller in this hybrid system, the results obtained from the modelling of this chiller are analyzed in this section. Figure 4 shows the effects of generator, evaporator and condenser temperatures on chiller performance coefficient. In this figure, the solid lines and the dashed lines indicate condenser temperatures of 33 and 39 ºC, respectively. According to this figure, the performance coefficient of the chiller increases with the rise of evaporator temperature and reduction of condenser temperature. For a specific evaporator temperature and condenser temperature, there is a minimum generator temperature at which the chiller performance coefficient is a maximum. As it is shown in Equation. (11), with the exchanged heat in the evaporator being constant, it can be concluded that the increase in performance coefficient is due to the reduction in the amount of exchanged heat in the absorption chiller generator. The results indicate that for the vaporization temperature of cooler in the ranges of 4-10 ºC and the working temperature of condenser in the range of 33-39 ºC, the maximum performance coefficient of the single-effect absorption chiller falls in the range of 0.75-0.81.

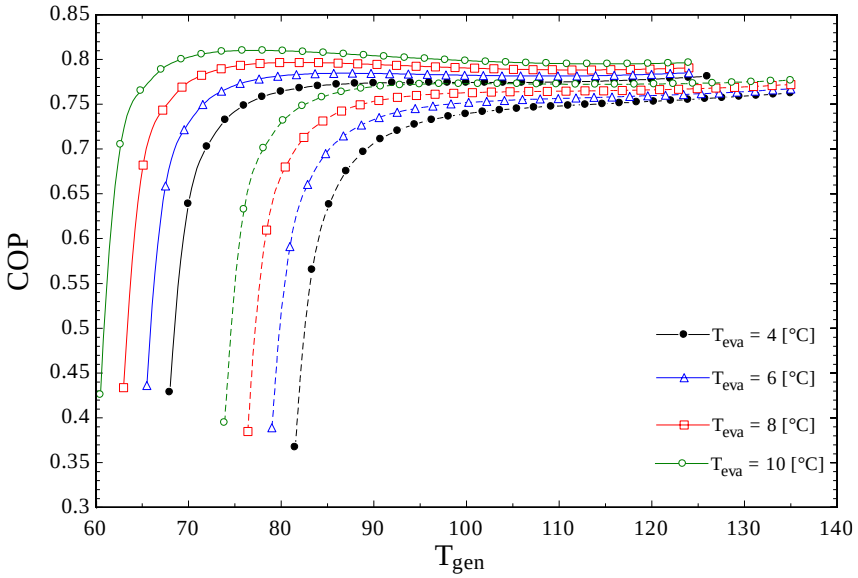

Figure 4. Performance coefficient of chiller versus generator temperature at condenser temperatures of 33 and 39 ºC.

Figure 5 shows the effects of generator and condenser temperatures on the amount of heat transfer in the cycle components. Solid lines and dashed lines indicate condenser temperatures of 33 and 39 ºC, respectively. As it is shown, in all the cases, the thermal load of the evaporator has not changed and has remained at constant values of 300 and 200 kW, respectively. The results indicate that the thermal loads of the generator and absorber diminish with the rise of generator temperature. There is a minimum generator temperature at which Q_{gen} and Q_{abs} have their minimum values; and if that temperature goes up, these two parameters keep their constant values. The results also show that there is little variation in the thermal load of condenser with respect to generator temperature. As it is observed in Figure 4, by raising the condenser temperature, the thermal loads of the generator and the

absorber are reduced. In achieving these results, the evaporator temperature has been assumed at 4 ºC.

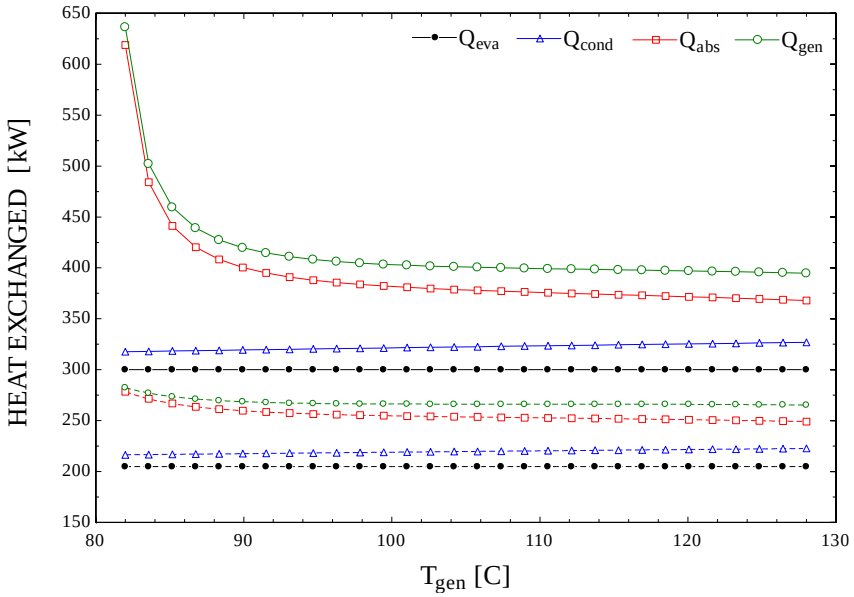

Figure 5. The thermal load of chiller components versus generator temperature at condenser temperatures of 33 and 39 ºC.

Parametric Analysis of the Hybrid System

In order to better understand the operating conditions of the examined hybrid system, the effects of different parameters on its performance have been analyzed in the following sections. Figures 6-9 show the effects of the molar flow rate of compressor inlet air on the overall efficiency of the hybrid system, fuel cell's working temperature and on the rates of exergy destruction and exergy loss in the hybrid system at three different compressor pressure ratios. It should be mentioned that in these analyses, the temperature of the hybrid system's exhaust gases has been assumed as 200 ºC.

The effect of the molar flow rate of hybrid system inlet air on system's overall efficiency has been illustrated in Figure 6. The overall efficiency refers to the efficiency of the combined cooling, heating and power system. As it is observed, with the increase in the flow rate of air entering the system, its overall efficiency diminishes. The main reason for this is the increase in the amount of work consumption by the air compressor and also the cooling of the fuel cell. As it is shown in Figure 7, the increase in the flow rate of system inlet air has a cooling effect on the fuel cell and reduces its working temperature. This, in turn, reduces the power output of the fuel cell and diminishes the efficiency of the hybrid system. The temperature of gases exiting the fuel cell cycle has a considerable influence on the performance of absorption chiller. By lowering the temperature of the exhaust gases from the fuel cell's afterburner, the amount of thermal energy transferred in the recuperators is reduced. This will lower the amount of heat entering the generator of the absorption chiller and substantially decrease the system's cooling load. Additionally, this will also reduce the thermal load of the heating system.

The findings indicate that the increase of compressor pressure ratio has little effect on the efficiency of the hybrid system. The increase of compressor pressure ratio not only

raises the temperature of exhaust gases from the compressor, but it also increases the amount of work consumption in the system. In this way, the increase of compressor pressure ratio will reduce the amount of electric power generated in the hybrid system and increase the amount of heat accumulated in the third and fourth recuperators. Such increases and decreases are almost equal, and this causes the overall efficiency of the system to remain constant.

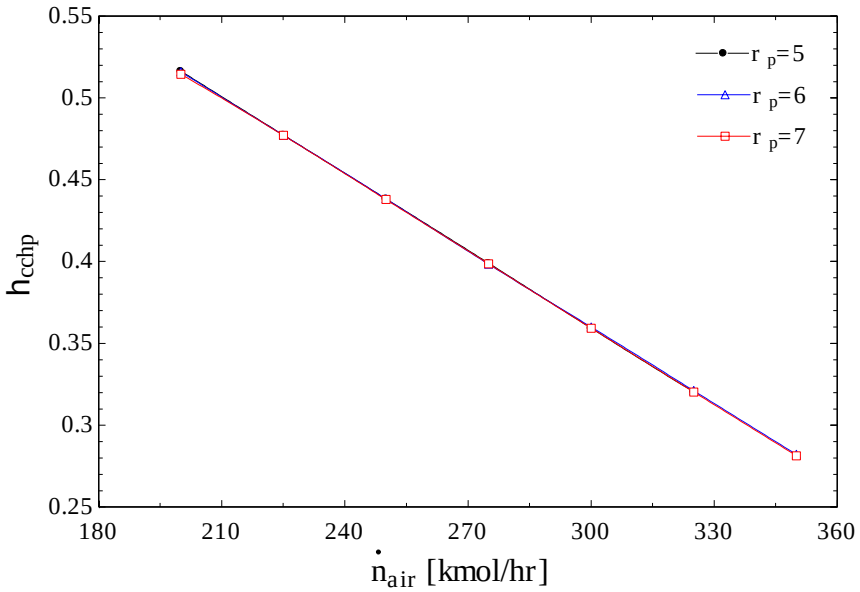

Figure 6. Molar flow rate of hybrid system inlet air versus overall system efficiency.

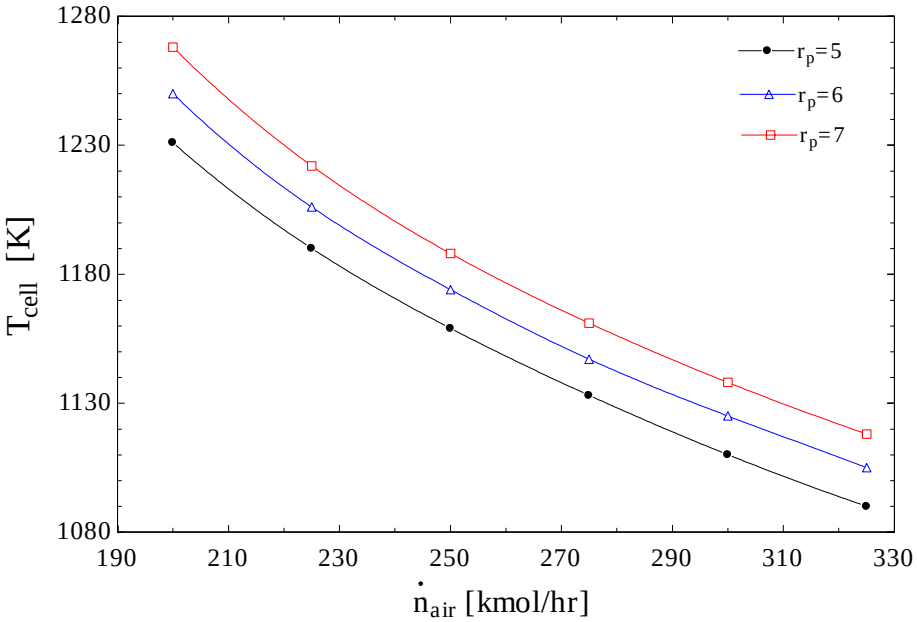

Figure 7. Molar flow rate of hybrid system inlet air versus the working temperature of fuel cell.

Figures 8 and 9 respectively display the effects of the molar flow rate of system inlet air on the rates of exergy destruction and exergy loss in the system. As it can be seen, the rates of exergy destruction and exergy loss in the system go up with the increase in the flow rate of system inlet air. This is mainly caused by the reduction in the sum of the electrical power and the heating and cooling loads generated in the system. Conversely, the investigations show that at a constant inlet air flow rate, the rates of exergy destruction and exergy loss in the system will go up by increasing the compressor pressure ratio. According to the obtained results, it is better to operate the introduced hybrid system at minimum working pressure and inlet air flow rate.

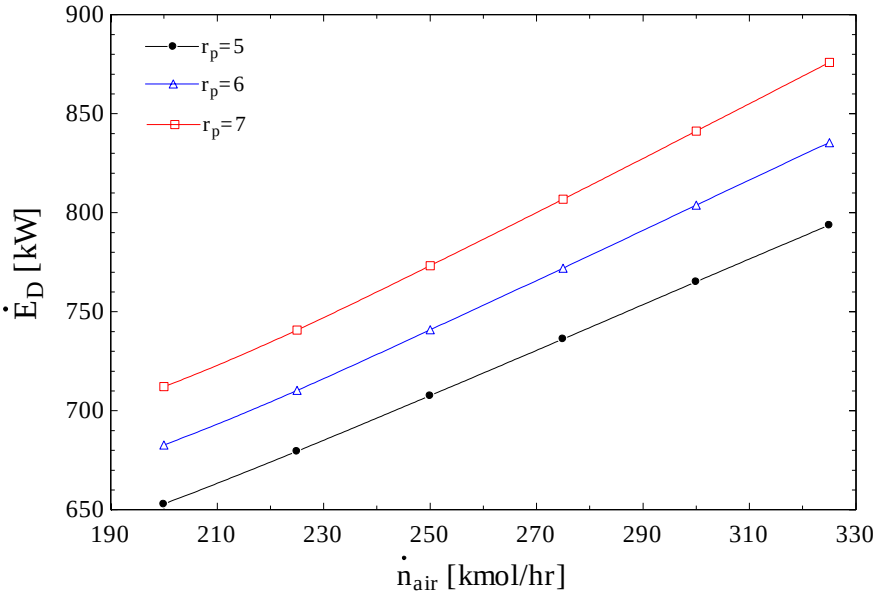

Figure 8. Molar flow rate of system inlet air versus rate of exergy destruction.

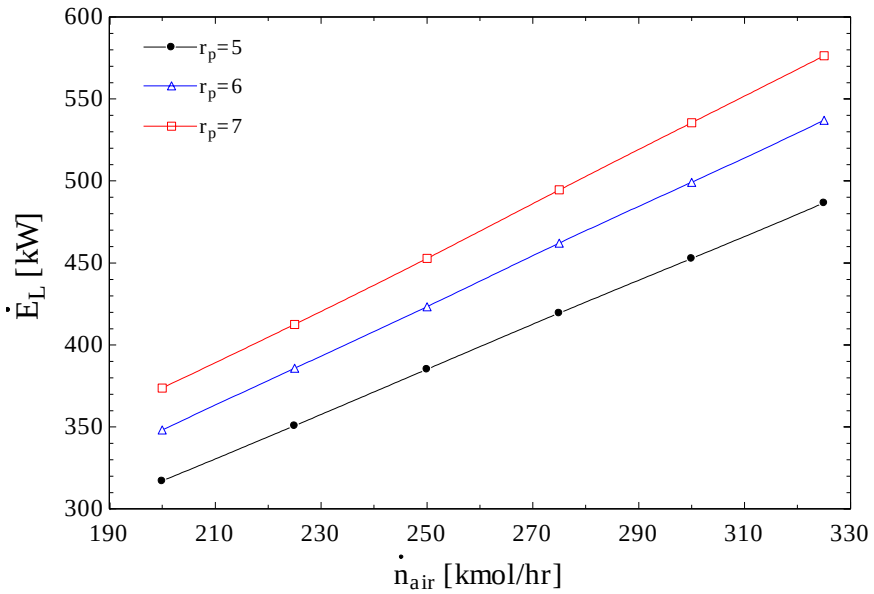

Figure 9. Molar flow rate of system inlet air versus rate of exergy loss.

In this section, the effect of the temperature of exhaust gases from the hybrid system stack has been studied by considering the parameters of system inlet air flow rate and compressor pressure ratio. Figure 10 shows the effect of the temperature of exhaust gases from the hybrid system on its overall efficiency. According to this figure, the overall efficiency of the system diminishes with the increase in the temperature of exhaust gases; and the main reason for this is the lack of sufficient heat absorption in the third and fourth recuperators and the reduction in the heating and cooling capacities of the hybrid system. As it is observed, an increase in the temperature of exhaust gases from 360 to 480 ºK will reduce the overall efficiency of the hybrid system by 15-20%. The results indicate that an increase in the system inlet air flow rate further cools the fuel cell and lowers the temperature of exhaust gases from it, thereby reducing the overall system efficiency. As it is shown, the maximum efficiency of the hybrid system is about 64%.

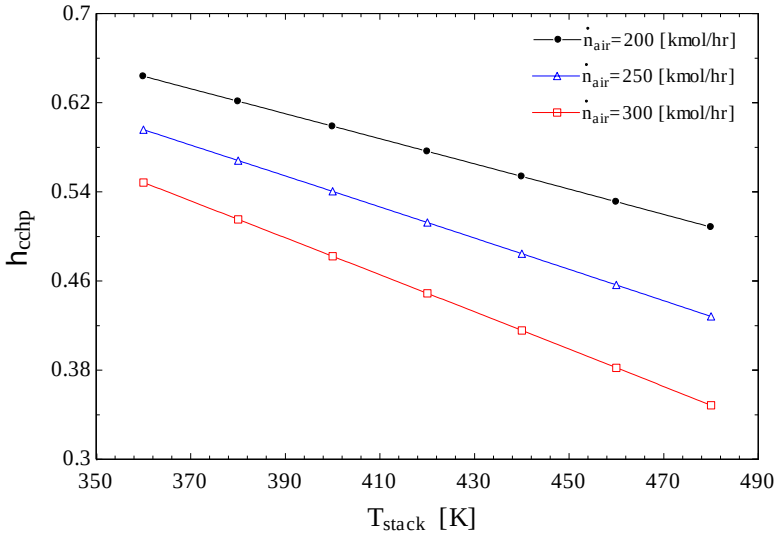

Figure 10. Temperature of exhaust gases from the hybrid system versus the overall system efficiency.

Figures 11 and 12 respectively illustrate the effects of the temperature of exhaust gases from the hybrid system stack on the rates of exergy destruction and exergy loss. As it is shown, with the rise in the temperature of exhaust gases, the rate of exergy destruction diminishes, while the rate of exergy loss increases. The main reason for the increased rate of exergy loss is the wasting of a large portion of thermal energy from the stack of the hybrid system. And the decline in the rate of exergy destruction is mainly due to the reduced level of heat transfer in system recuperators.

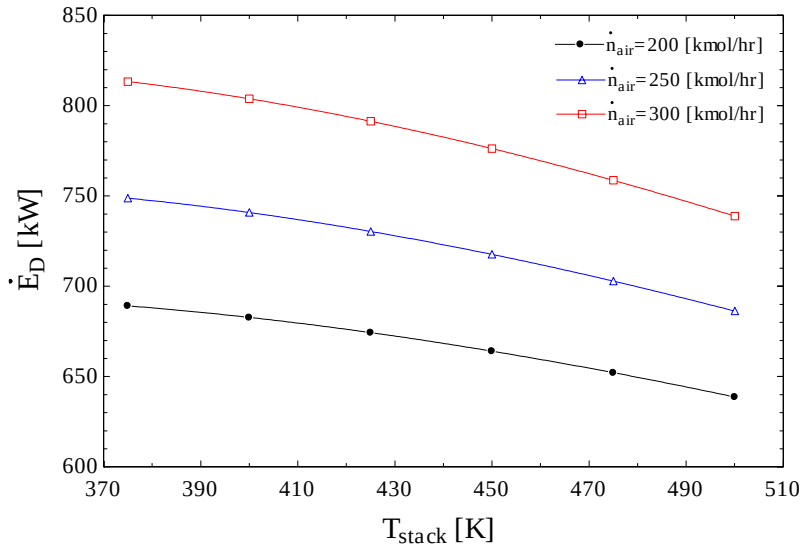

Figure 11. Temperature of exhaust gases from the hybrid system versus the rate of exergy destruction.

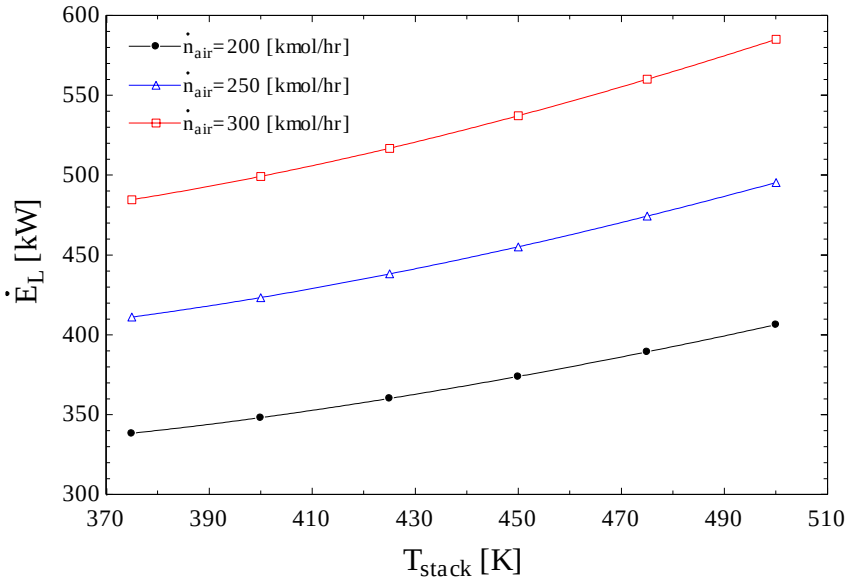

Figure 12. Temperature of exhaust gases from the hybrid system versus the rate of exergy loss.

Figure 13 shows the effect of the temperature of exhaust gases from the hybrid system on its overall efficiency at three different pressure ratios. As observed, the rise in the system's working pressure doesn't have a significant influence on the overall efficiency of the hybrid system; and for the three different working pressures, the same reduction of system efficiency can be seen with the rise in the temperature of exhaust gases.

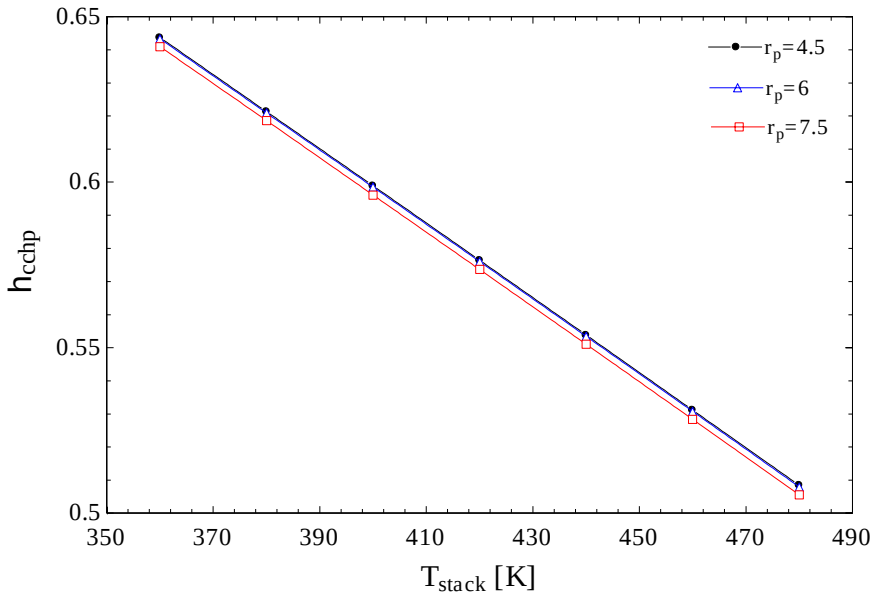

Figure 13. Temperature of exhaust gases from the hybrid system versus overall system efficiency at three different pressure ratios.

By examining the results obtained from the different working conditions of the hybrid system, the output results of the system in the optimal state have been extracted and reported in Table 3. In this condition, the temperature of exhaust gases is 400 K, compressor pressure ratio is 4.5, and the molar flow rate of compressor inlet air is 200 kmole/h.

Table 3. Different performance parameters of the hybrid system in the optimal operating conditions.

Parameter	**Assumed value**
Fuel cell temperature [K]	1221
Absorber temperature [K]	306
Condenser temperature [K]	306
Generator temperature [K]	348
Evaporator temperature [K]	285
Q_{eva} [kW]	205
COP	0.8245
Net generated power (kW)	402
Electrical efficiency (%)	24.74
Thermal efficiency (%)	19.34
Total efficiency (%)	44.09
Exergy efficiency (%)	59.89

The reduction of entropy generation in heating systems is an important issue and should be investigated. Figure 14 shows the variation of entropy generation rate for each component of the absorption chiller. As it is observed, the highest entropy generation rate belongs to the generator and then the absorber, and the lowest rate is associated with the pressure-reducing valve between the evaporator and the condenser. Also, Figure 15 displays the exergy destruction rate for each chiller component. Similar to the entropy generation rate, the highest exergy destruction rate occurs in the generator, and the lowest rate in the pressure-reducing valve between the evaporator and the condenser.

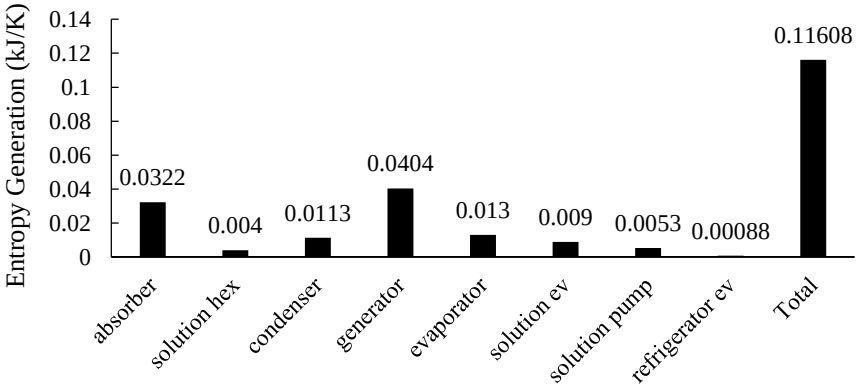

Figure 14. Variations of entropy generation rate in chiller components.

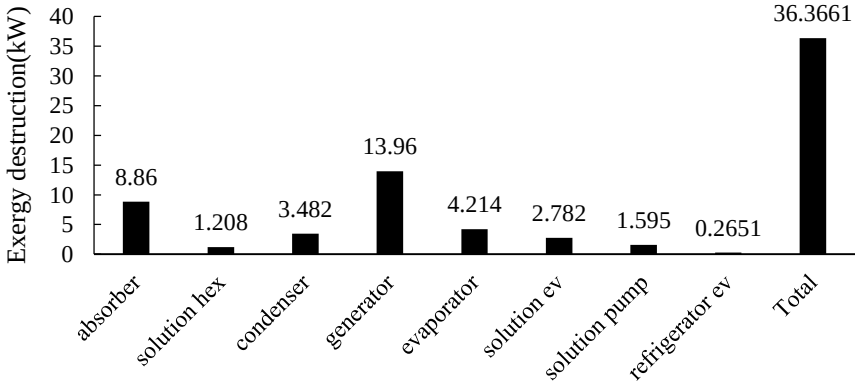

Figure 15. Variations of exergy destruction rate in chiller components.

We now discuss the rates of entropy generation and exergy destruction in the fuel cell cycle. As it is observed in Figures 16 and 17, the highest entropy generation rate occurs in the fuel cell, and the highest exergy destruction rate in the heat exchanger for fuel cell inlet air. The findings also show that the lowest rates of entropy generation and exergy destruction occur in the two water pumps. The results indicate that the fuel cell cycle has greater entropy generation and exergy destruction rates than the chiller cycle.

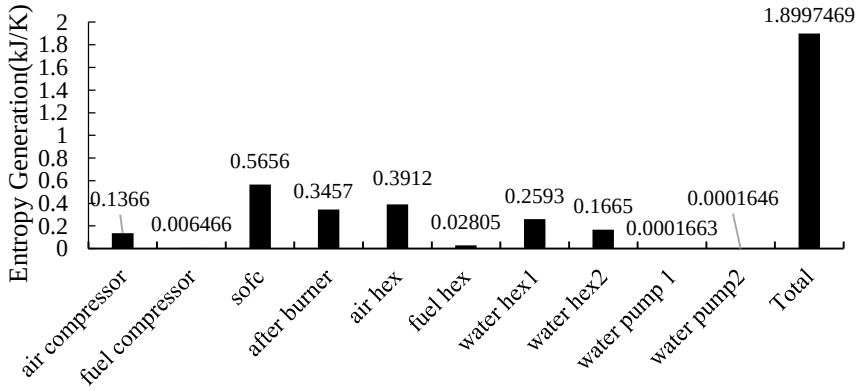

Figure 16. Variations of entropy generation rate in the components of fuel cell cycle.

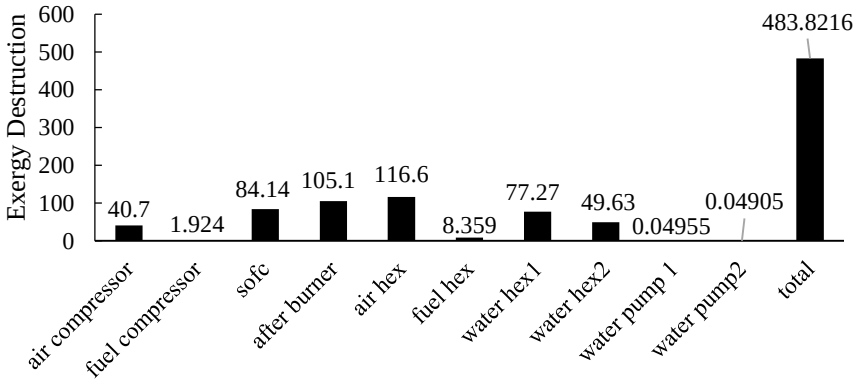

Figure 17. Variations of exergy destruction rate in the components of fuel cell cycle.

CONCLUSIONS

The findings of the present research have been summarized as follows:

- The performance coefficient of the chiller increases with the rise of evaporator temperature and the reduction of condenser temperature. For a specific evaporator temperature and condenser temperature, there is a minimum generator temperature at which the chiller performance coefficient is maximized. The results show that for an evaporation temperature of coolant in the range of 4-10 ºC and working temperature of condenser in the range of 33-39 ºC, the minimum performance coefficient for the single-effect absorption chiller is in the range of 0.7-0.81.
- By increasing the flow rate of air entering the system, its overall efficiency is reduced. This mainly occurs due to the increase in the amount of work done by the air compressor and also the cooling of the fuel cell. With the rise in the flow rate of system inlet air, the rates of exergy destruction and exergy loss in the system increase.

- Increasing the working pressure of the system has little effect on the efficiency of the hybrid system; and for all the three working pressures, the same efficiency reduction is achieved by raising the temperature of exhaust gases.
- The overall efficiency of the hybrid system diminishes with the rise in the temperature of exhaust gases. The main cause of this is insufficient heat absorption in the third and fourth recuperators and the reduction in the heating and cooling capacities of the hybrid system. The findings indicate that by increasing the temperature of exhaust gases from 360 to 480 K, the overall efficiency of the hybrid system is reduced by 15-20%. With the rise in the temperature of exhaust gases, the rate of exergy destruction in the hybrid system diminishes, while the rate of exergy loss increases. The main reason for the increase in the rate of exergy loss is the wasting of a large portion of thermal energy from the stack of the hybrid system.
- The findings related to the absorption chiller show that the highest entropy generation rate occurs in the generator followed by the absorber, and the lowest rate takes place in the pressure-reducing valve between the evaporator and the condenser. Also, the highest exergy destruction rate occurs in the generator, and the lowest rate in the pressure-reducing valve between the evaporator and the condenser.
- The results related to the fuel cell cycle indicate that the highest entropy generation rate occurs in the fuel cell, and the highest exergy destruction rate takes place in the heat exchanger for fuel cell inlet air. The findings also show that the lowest rates of entropy generation and exergy destruction occur in the two water pumps.
- The results indicate that the fuel cell cycle has greater entropy generation and exergy destruction rates than the chiller cycle.

REFERENCES

[1] Onovwiona HI, Ugursal VI. Residential cogeneration systems: review of the current technology. Renewable and Sustainable Energy Reviews. 2006; 10(5): 389-431.

[2] Liu M, Shi Y, Fang F. Combined cooling, heating and power systems: A survey. Renewable and Sustainable Energy Reviews. 2014; 35: 1–22.

[3] Pirkandi J, Ghassemi M, Hamedi MH, Mohammadi R. Electrochemical and thermodynamic modeling of a CHP system using tubular solid oxide fuel cell (SOFC-CHP). Journal of Cleaner Production. 2012; 29-30: 151-162.

[4] Buonomano A, Calise F, Dentice d'Accadia M, Palombo A, Vicidomini M. Hybrid solid oxide fuel cells–gas turbine systems for combined heat and power: A review. Journal of Applied Energy. 2015; 156:32–85.

[5] Velumani S, Guzmán CE, Peniche R, Vega R. Proposal of a hybrid CHP system: SOFC/microturbine/absorption chiller. International Journal of Energy Research 2010; 34:1088–1095.

[6] Ozcan H, Dincer I. Thermodynamic analysis of an integrated SOFC, solar ORC and absorption chiller for tri-generation applications. Fuel Cells. 2013; 13:781–93.

[7] Ranjbar F, Chitsaz A, Mahmoudi SMS, Khalilarya S, Rosen M. Energy and exergy assessments of a novel trigeneration system based on a solid oxide fuel cell. Energy Conversion and Management. 2014; 87: 318-327.

[8] Zhao H, Ting Jiang T, Hou H. Performance analysis of the SOFC-CCHP system based on H2O/Li-Br absorption refrigeration cycle fueled by coke oven gas. Energy. 2015; 91: 983-993

[9] Chitsaz A, Mehr AS, Mahmoudi SMS., Exergoeconomic analysis of a trigeneration system driven by a solid oxide fuel cell. Energy Conversion and Management. 2015; 106: 921–931.

[10] Moussawi H, Fardouna F, Louahlia H. 4-E based optimal management of a SOFC-CCHP system model for residential applications. Energy Conversion and Management. 2017; 151: 607–629.

[11] Jing R, Wang M, Brandon N, Zhao Y. Multi-criteria evaluation of solid oxide fuel cell based combined cooling heating and power (SOFC-CCHP) applications for public buildings in China. Energy. 2017; 141: 273-289.

[12] Jing R, Wang M, Wang W, Brandon N, Li N, Chen J, Zhao Y. Economic and environmental multi-optimal design and dispatch of solid oxide fuel cell based CCHP system. Energy Conversion and Management. 2017; 154: 365–379.

[13] Hou Q, Zhao H, Yang X. Thermodynamic performance study of the integrated MR-SOFC-CCHP system. Energy. 2018; 150: 434-450.

[14] Gomri R. Second law comparison of single effect and double effect vapor absorption refrigeration systems. Energy Conversion and Management. 2009;50: 1279–1287.

[15] Pirkandi J, Mahmoodi M, Ommian M. Thermo-economic performance analysis of a gas turbine generator equipped with a pressurized and an atmospheric solid oxide fuel cell. Energy Conversion and Management. 2017; 136: 249-261.